



University of  
New Haven

University of New Haven  
**Digital Commons @ New Haven**

---

Fire Science and Professional Studies Faculty  
Publications

Fire Science and Professional Studies

---

11-20-2015

# Enhanced Thermal Decomposition Kinetics of Poly(lactic acid) Sacrificial Polymer Catalyzed by Metal Oxide Nanoparticles

Lu Liu

*University of Maryland - College Park*

Michael R. Zachariah

*University of Maryland - College Park*

Stanislav I. Stoliarov

*University of Maryland - College Park*

Jing Li

*University of New Haven, jli@newhaven.edu*

Follow this and additional works at: <http://digitalcommons.newhaven.edu/firescience-facpubs>



Part of the [Emergency and Disaster Management Commons](#)

---

## Publisher Citation

Liu, L., M. R. Zachariah, S. I. Stoliarov and J. Li (2015). "Enhanced thermal decomposition kinetics of poly(lactic acid) sacrificial polymer catalyzed by metal oxide nanoparticles." RSC Advances 5(123): 101745-101750.

## Comments

This is the author's accepted manuscript of the article published in RSC Advances. The final version can be found at <http://dx.doi.org/10.1039/CSRA19303F>

1 **Enhanced thermal decomposition kinetics of Poly (Lactic Acid)**  
2 **sacrificial polymer catalyzed by metal oxide nanoparticles**

3 Lu Liu<sup>a</sup>, Michael R. Zachariah<sup>\*ab</sup>, Stanislav I. Stoliarov<sup>c</sup>, Jing Li<sup>\*d</sup>

4 a. Department of Chemistry and Biochemistry, University of Maryland, College Park, MD 20742, USA

5 b. Department of Chemical and Biomolecule Engineering, University of Maryland, College Park, MD 20742,  
6 USA

7 c. Department of Fire Protection Engineering, University of Maryland, College Park, MD 20742, USA

8 d. Department of Fire Science & Professional Studies, University of New Haven, West Haven, CT, 06516, USA

9 Tel.: +01-203-932-1197; Fax: +01-203-931-6095 E-mail address: jli@newhaven.edu (J. Li).

---

10 **ABSTRACT:** Poly Lactic Acid (PLA) has been used as sacrificial polymer in the fabrication of  
11 battery separators and can be employed in 0D-3D Vaporization of a Sacrificial Component (VaSC)  
12 fabrication. In this study, 1wt% PLA/Fe<sub>2</sub>O<sub>3</sub>, PLA/CuO, PLA/Bi<sub>2</sub>O<sub>3</sub> composites are prepared by  
13 solvent evaporation casting. Scanning Electron Microscopy (SEM) images indicate that the  
14 embedded nanoparticles are well dispersed in the polymer matrix and X-Ray Diffraction (XRD)  
15 verifies the crystallinity of these Metal Oxides (MOs). Thermal stability analysis of PLA and  
16 PLA/MO composites is performed using a Thermogravimetric Analyzer (TGA) and Differential  
17 Scanning Calorimeter (DSC). The overall heat of combustion is measured by Microscale  
18 Combustion Calorimetry (MCC) and is found to be insensitive to the presence of nanoparticles.  
19 The overall catalytic effects of the three metal oxides trends as: Bi<sub>2</sub>O<sub>3</sub>>Fe<sub>2</sub>O<sub>3</sub>>CuO ≈ inert  
20 material. PLA/Bi<sub>2</sub>O<sub>3</sub> decomposition onset temperature (T<sub>5%</sub>) and maximum mass loss

21 decomposition temperature ( $T_{\max}$ ) are lowered by approximately 75 K and 100 K respectively  
22 compared to the neat PLA. The as-synthesized  $\text{Bi}_2\text{O}_3$  is identified as the most effective additive  
23 among those proposed in the literature to catalyze the PLA thermal decomposition process. A  
24 numerical pyrolysis modeling tool, ThermaKin, is utilized to analyze thermogravimetric data of  
25 all the PLA/MOs and to produce a description of the decomposition kinetics, which can be utilized  
26 for modeling of thermal vaporization of these sacrificial materials.

---

27

## 28        1. Introduction

29            Poly Lactic Acid (PLA) is an environmentally friendly polymer produced from plants  
30 (mainly from starch and sugar) including corn, potatoes and sugar-beets, and has attracted attention  
31 for its biocompatibility, biodegradability, and thermoplastic processability.<sup>1</sup> It has been reported  
32 that the greenhouse gas emission rate of PLA is approximately 1600 kg CO<sub>2</sub>/metric ton, while that  
33 of polypropylene (PE), polystyrene (PS), polyethylene terephthalate (PET), and nylon are 1850,  
34 2740, 4140, and 7150 kg CO<sub>2</sub>/metric ton, respectively.<sup>2</sup> Further, PLA's low temperature of thermal  
35 degradation with minimal solid residue (gasified lactide) has made it an attractive candidate as a  
36 sacrificial component in polymer fabrication.<sup>2-4</sup>

37            PLA is also one of the two major plastics explored as 3D printing inks (the other being  
38 Acrylonitrile Butadiene Styrene (ABS)) because of its thermoplastic properties.<sup>5</sup> Although ABS is  
39 currently the dominant 3D printing polymer, PLA offers the advantage of bio-compatibility. As a  
40 sacrificial component, PLA can be 3D printed to create complex-shaped molds<sup>6-8</sup>. For example,  
41 White *et al.*<sup>7</sup> have fabricated PLA as spheres (0D), fibers (1D), sheets (2D), and 3D printed  
42 sacrificial materials, leaving behind the reverse replica. Pitet *et al.*<sup>9</sup> have explored PLA as a  
43 sacrificial component in copolymers to create porous membranes for battery separators utilizing the  
44 fact that its decomposition temperature is about 200°C lower than thermally stable polymers such  
45 as polyimide (PI), epoxies, Poly(vinylidene fluoride-hexafluoropropylene) (PVDF-HFP), *etc.* The  
46 decomposition of neat PLA occurs above ~550K, which can lead to the thermal instability of other  
47 polymer blends in practical applications during prolonged heat treatment<sup>7</sup>. Therefore, alkali earth  
48 metal oxides<sup>3</sup>, rare metal (scandium (III) triflates (CF<sub>3</sub>SO<sub>3</sub>-))<sup>10</sup>, and tin-containing compounds<sup>7, 8, 11</sup>  
49 were studied as catalysts for PLA thermal decomposition. Moore *et al.*<sup>6, 7</sup> added Sn-based reactants  
50 to lower the decomposition temperature by 90 K to effectively remove sacrificial PLA at a lower

51 temperature while avoiding thermal damage to the epoxy mold. It was found that the same amount  
52 of SnO<sub>x</sub> additive works even better than tin (II) octoate to further reduce the total decomposition  
53 time at the same temperature.<sup>7</sup> Mori *et al.* reported similar results using Sn-based compounds and  
54 recognized that these catalysts could enhance the breakage of ester bonds in the polymer backbone,  
55 thus promoting the fragmented polymer ends to experience chain backbiting and transesterification  
56 reactions before further depolymerization.<sup>11</sup> Almost all of the previous studies used a high loading  
57 of more than 5 wt% catalyst.<sup>3, 6-11</sup>

58 Addition of catalysts into PLA is usually achieved by surface treatment (including  
59 impregnation or solvent swelling)<sup>6</sup>, solvent evaporation casting<sup>7</sup>, or vane extruding.<sup>12</sup> Dong *et al.*<sup>6</sup>  
60 utilized solvent swelling to immobilize metal ions (tin (II) octoate solution) into PLA fibers. Later,  
61 Moore *et al.* used solvent evaporation to imbed SnO<sub>x</sub> into PLA, further decreasing the  
62 decomposition temperature.<sup>7</sup> Solvent evaporation casting of PLA with specific viscosity was  
63 utilized by Guo *et al.* in a proposed 3D printing ink drying technique.<sup>13, 14</sup> Zhang *et al.* utilized  
64 melt blending with a vane extruder with heating to get mono-dispersed PLA/TiO<sub>2</sub>  
65 nanocomposites.<sup>12</sup>

66 It is widely known that controlling the removal process of the sacrificial materials is extremely  
67 difficult, requiring carefully designed thermal conditions and perfect timing to fully eliminate the  
68 sacrificial material at minimal cost, while also keeping the host material undamaged.<sup>15, 16</sup>  
69 Therefore, catalysts are added to increase the decomposition temperature difference between the  
70 sacrificial materials and host materials to maintain the integrity of the host polymer.<sup>3, 6-11</sup> Usually  
71 the removal time for even nano-scale channels are hours to days and are highly non-linear relative  
72 to different heating conditions, which makes the control process hard to predict.<sup>6, 7, 15</sup> The severity  
73 of this problem increases as larger and more complex geometries are required with the rapid

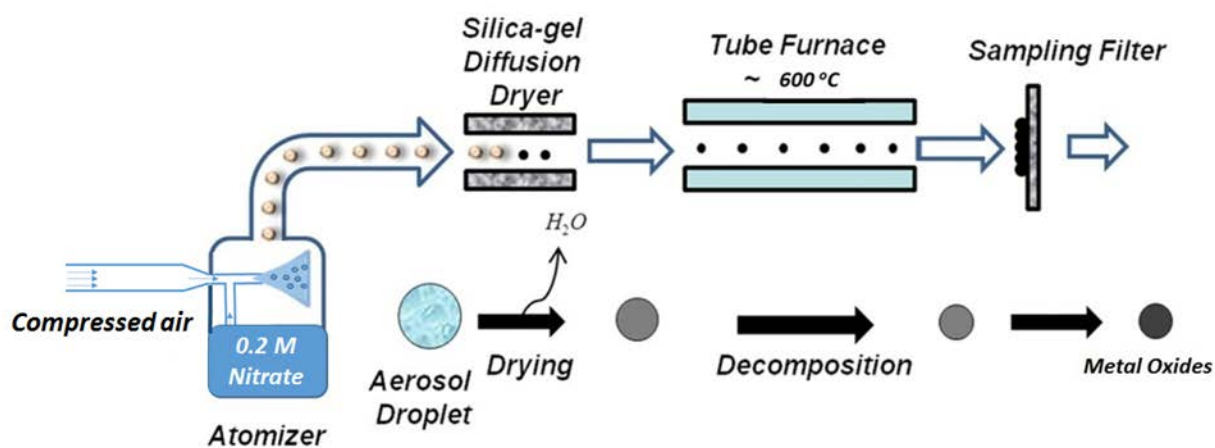
74 development of 3D printing using such sacrificial materials.<sup>13, 14</sup> MOs have not been studied  
75 extensively as catalysts for PLA, especially at small loadings ( $< 5\%$ )<sup>3,6,11</sup>.

76 In this work, we employed 1 wt% MOs loading to study the catalytic effects of MOs. Bi<sub>2</sub>O<sub>3</sub>,  
77 CuO and Fe<sub>2</sub>O<sub>3</sub> are synthesized by spray pyrolysis<sup>17-19</sup> and then uniformly embedded into PLA  
78 matrix using solvent evaporation casting. XRD and SEM are performed to verify the additives'  
79 crystallinity and homogenous dispersion in the PLA matrix. The thermal properties of PLA/MOs  
80 composites relative to neat PLA are measured by TGA (Thermogravimetric Analyzer), DSC  
81 (Differential Scanning Calorimeter), and MCC (Microscale Combustion Calorimeter) to examine  
82 the MOs catalytic effect on the PLA's thermal degradation process and overall combustion heat.  
83 Thermal degradation simulations are performed to fit the experimental TGA curve with a number  
84 of first order chemical pyrolysis reaction models using a one dimensional pyrolysis model (-  
85 ThermaKin<sup>20</sup> running under thermally thin mode). This kinetic fitting work is preformed to  
86 reproduce the TGA data, which provides kinetic fundamentals to potentially further predict and  
87 control the removing process time and temperatures of PLA/MOs for different geometries or  
88 length scales in various heating environments in the future.

## 89 **2. Experimental**

90 All metal oxide additives are in-house synthesized by aerosol spray pyrolysis.<sup>17-19</sup> The spray  
91 pyrolysis system (pictured in Figure 1) consists of an atomizer (to produce aerosol droplets), a  
92 silica-gel diffusion drier (to remove solvent), an isothermal furnace (to decompose precursor  
93 droplets), and a stainless steel sample collector with 0.4  $\mu\text{m}$  DTTP Millipore filter (to collect  
94 nanoparticles). The aerosol droplets of precursor solution are generated using a collision-type  
95 nebulizer with an initial droplet diameter of approximately 1 $\mu\text{m}$ , which is then desiccated by  
96 passing through the silica-gel diffusion dryer. The dehydrated aerosol precursors then decompose

97 into the solid metal oxide particles in the tube furnace set at 600 °C for Fe<sub>2</sub>O<sub>3</sub> and CuO, or 1050°C  
98 for Bi<sub>2</sub>O<sub>3</sub>, with a residence time of about 1s. Particles exiting the aerosol reactor are then collected  
99 on a 0.4 μm pore size DTTP Millipore filter with 10%-20% porosity (EMD Millipore). The  
100 precursors used for the Bi<sub>2</sub>O<sub>3</sub>, Fe<sub>2</sub>O<sub>3</sub>, and CuO are Bi(NO<sub>3</sub>)<sub>3</sub>·5H<sub>2</sub>O, Fe(NO<sub>3</sub>)<sub>3</sub>·9H<sub>2</sub>O and  
101 Cu(NO<sub>3</sub>)<sub>2</sub>·3H<sub>2</sub>O respectively, all from Sigma-Aldrich. A total precursor concentration of 0.200 M  
102 aqueous solution is used for MOs, and to dissolve Bi(NO<sub>3</sub>)<sub>3</sub>·5H<sub>2</sub>O, 1:5 concentrated nitric acid  
103 and water mixture is used as the solvent. The aerosol spray pyrolysis is a droplet to droplet method,  
104 and the formation mechanism of MOs is described in Figure 1 below. Lognormal poly-dispersed  
105 spherical solid particles are generated e.g. the Fe<sub>2</sub>O<sub>3</sub> particles are spherical particles with a  
106 lognormal distribution peak at 84nm.<sup>19</sup>



107

108 **Figure 1.** Aerosol spray pyrolysis synthesis system for metal oxides.

109 PLA (Rejuven8 Plus Spartech) is obtained from Nature Works and used as received. The  
110 PLA sheets are 0.7 mm thick and cut into small pieces for solvent evaporation casting. 1.000 g  
111 PLA is first dissolved in 100.0 mL CH<sub>2</sub>Cl<sub>2</sub> with magnetic stirring for 30 mins. Then 10.0 mg (1 wt%)  
112 MO is added to the solution and ultra-sonicated for 1h. The solutions are then poured onto a watch  
113 glass and dried in a 50 °C convection oven to for 12h. Thin films of neat PLA (baseline reference)

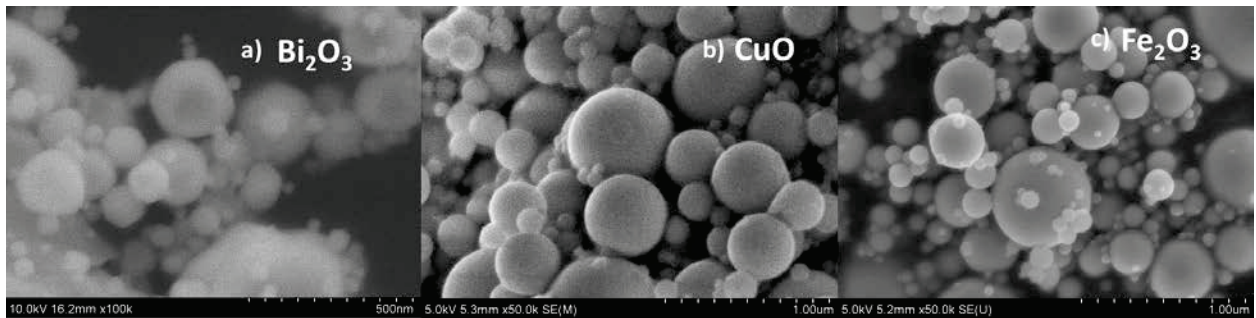
114 and PLA/MO composites are obtained after solvent evaporation. Small pieces of the as prepared  
115 thin films were then used for the thermal tests. Crystal structures of metal oxides are characterized  
116 by XRD with a Bruker Smart1000 using Cu K $\alpha$  radiation. SEM results were obtained by Hitachi  
117 SU-70 SEM. For cross-sectional SEM images, samples are first fractured in liquid nitrogen and  
118 then sputter-coated with carbon. Nitrogen (N<sub>2</sub>) adsorption-desorption isotherms and Brunauer–  
119 Emmett–Teller (BET) surface were measured at 77 K with an Micromeritics ASAP 2020  
120 Porosimeter.

121 A Netzsch F3 Jupiter Simultaneous Thermal Analyzer (STA), employed in the thermal stability  
122 study, combines a TGA equipped with a 1  $\mu$ g-resolution microbalance and DSC heat flow  
123 measurement with a steel furnace. Thus the STA can measure the TGA and DSC signals  
124 simultaneously during a single experiment. The PLA/MOs films were stored in a desiccator for 48  
125 hours prior to testing, and then cut and pressed into Platinum-Rhodium crucibles with ventilation  
126 lids with a sample mass of 6-7 mg. The thermal decomposition experiments were performed at a  
127 heating rate of 10 K min<sup>-1</sup> from 40 °C to 600 °C under 99.999% (UHP) N<sub>2</sub> at a flow rate of 50  
128 cm<sup>3</sup>·min<sup>-1</sup>. A microscale combustion calorimeter (MCC) with 3 mg samples was used to measure  
129 the heat release rate and total heat of combustion.<sup>1</sup> The MCC combines a condensed phase  
130 pyrolyzer and gas phase combustor. The samples are first decomposed in 80 cm<sup>3</sup> min<sup>-1</sup> UHP N<sub>2</sub>  
131 flow, 60 K min<sup>-1</sup> heating rate from 75 to 600 °C inside the pyrolyzer, which is similar to the STA  
132 furnace, and then transferred to the combustor where the gaseous fuel (decomposition products)  
133 was burned at 950 °C to ensure complete combustion mixing with additional 20 cm<sup>3</sup>·min<sup>-1</sup> O<sub>2</sub>. The  
134 entire experimental measurement of HRR (Heat Release Rate) followed ASTM standard ASTM  
135 D 7309-13.<sup>21</sup> The heat release rate was measured based on Thornton's rule by measuring the O<sub>2</sub>  
136 consumption rate of combustion.<sup>22</sup>



137 **3. Results and Discussion**

138 Figure 2 shows the SEM micrographs of spray pyrolysis synthesized Bi<sub>2</sub>O<sub>3</sub>, Fe<sub>2</sub>O<sub>3</sub> and CuO  
139 nanoparticles, which are solid spherical particles with diameters from 50nm to 1µm following a  
140 log normal distribution with a peak (Fe<sub>2</sub>O<sub>3</sub> at 84 nm<sup>19</sup>, CuO at 86nm and Bi<sub>2</sub>O<sub>3</sub> at 87 nm, shown  
141 in Figure S1). Figure S2 shows BET surface area results: Fe<sub>2</sub>O<sub>3</sub>-13 m<sup>2</sup>/g, CuO-23 m<sup>2</sup>/g, Bi<sub>2</sub>O<sub>3</sub>-4  
142 m<sup>2</sup>/g, with Bi<sub>2</sub>O<sub>3</sub> surface area being the lowest, indicating that surface area does not explain the  
143 superior catalytic activity of Bi<sub>2</sub>O<sub>3</sub>. The crystal structure of oxides are investigated from XRD  
144 shown in Figure S3. All peaks in Fe<sub>2</sub>O<sub>3</sub> can be indexed to γ-Fe<sub>2</sub>O<sub>3</sub> phase (JCPDS card No.: 39-  
145 1346); Bi<sub>2</sub>O<sub>3</sub> with JCPDS card No.: 27-0050, while CuO peaks corresponds to tenorite with  
146 JCPDS card No.: 48-1548.



148 **Figure 2.** SEM of nanoparticles a) Bi<sub>2</sub>O<sub>3</sub>, b) CuO, c) Fe<sub>2</sub>O<sub>3</sub>, prepared from spray pyrolysis.

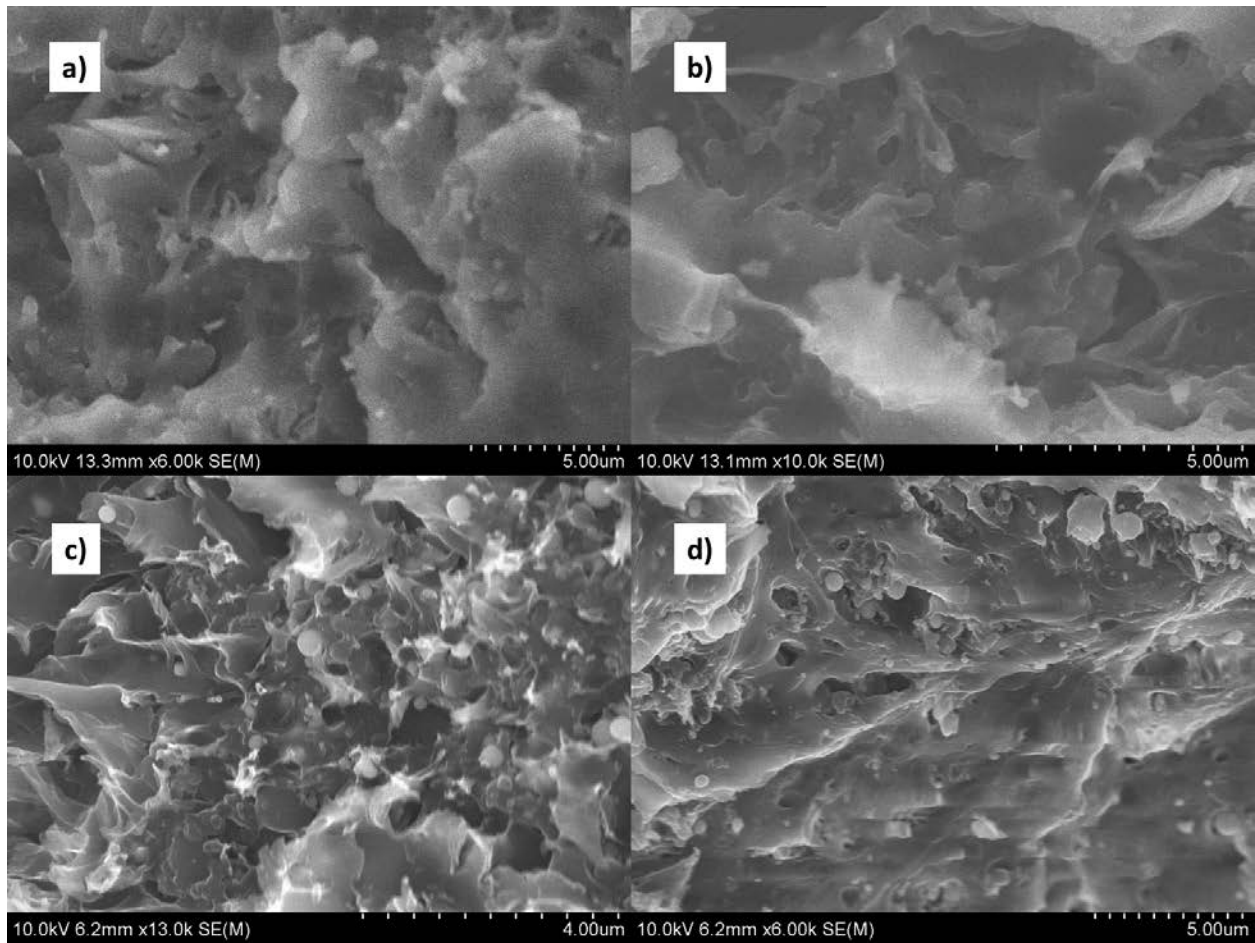
149 It is widely known that the dispersion of nanoparticles in polymer will greatly influence  
150 the both chemical and physical properties of the PLA/MO composites. Homogeneous dispersion  
151 of MO nanoparticles will affect the thermal and mechanical behaviors of PLA, such as wettability,  
152 UV transmittance, strength and ductility, elasticity, viscosity, antibacterial property.<sup>12</sup>

153 Cross-sectional SEM images are taken to check the dispersion of MOs in the composites.  
154 PLA/MOs are first fractured in liquid nitrogen and then broken off for cross-sectional images.

155 Figure 3a) and 3b) show neat PLA cross-sectional image without particles, and Figure 3c) and 3d)  
156 are PLA/Fe<sub>2</sub>O<sub>3</sub>, PLA/CuO films images, respectively. It is clear from these images that all  
157 nanoparticles are well dispersed in the PLA films. Figure 4 shows the cross-sectional PLA/Bi<sub>2</sub>O<sub>3</sub>  
158 structure, and it is clear that spherical Bi<sub>2</sub>O<sub>3</sub> are uniformly dispersed in PLA and un-aggregated.  
159 The film is about 50 μm thick, indicated by low magnification image of Figure 4a) and Figure 4b).  
160 Moreover, Figure 4c) and 4d) give a closer view of the cross-sections, all showing that particles  
161 are coated and/or connected by PLA while separated from other nanoparticles.

162

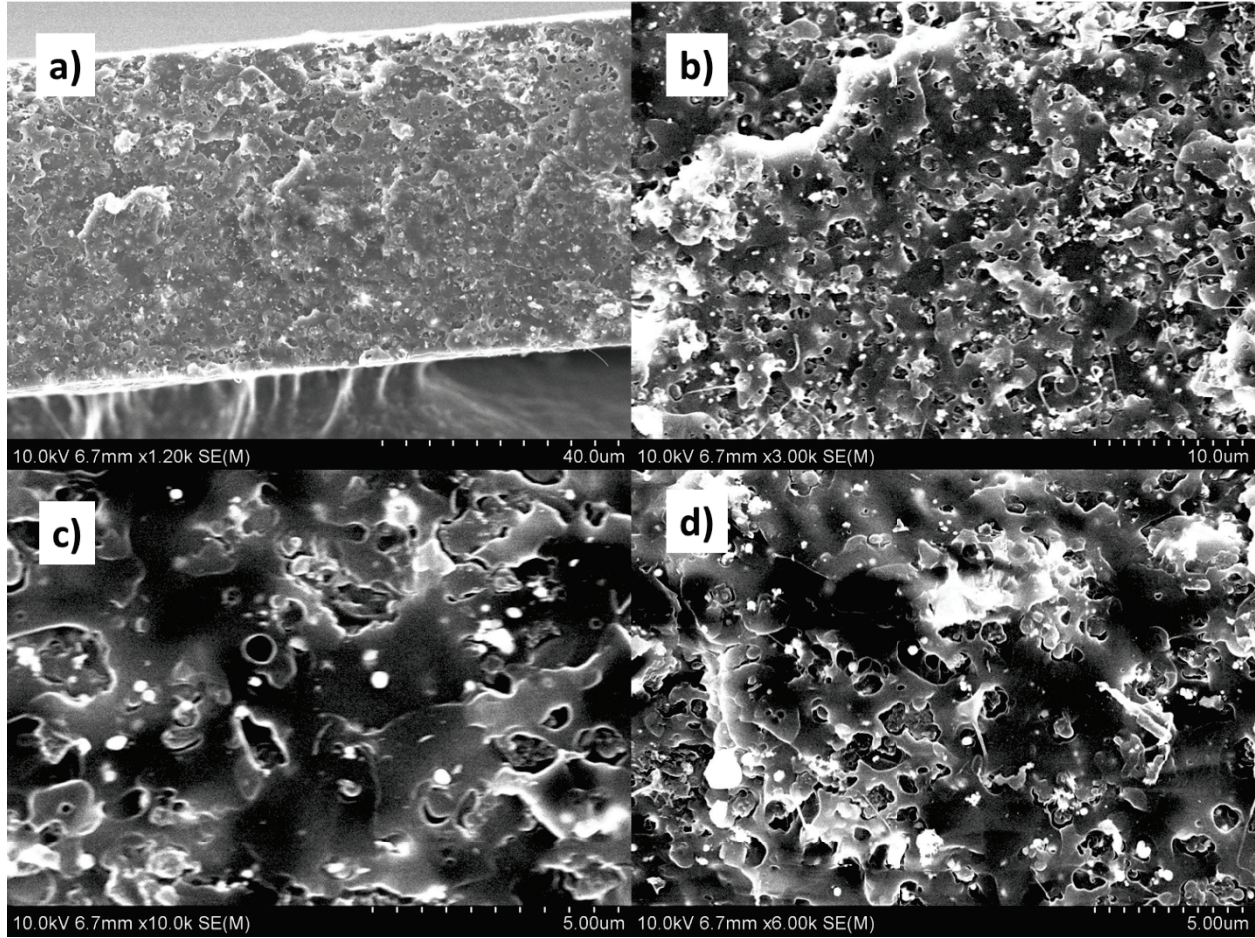
163



164

165

**Figure 3.** SEM of cross-sectioned a) and b) PLA, c) PLA/Fe<sub>2</sub>O<sub>3</sub>, d) PLA/CuO films.



166

167

**Figure 4.** SEM of cross-sectioned PLA/Bi<sub>2</sub>O<sub>3</sub> film.

168

169

170

171

172

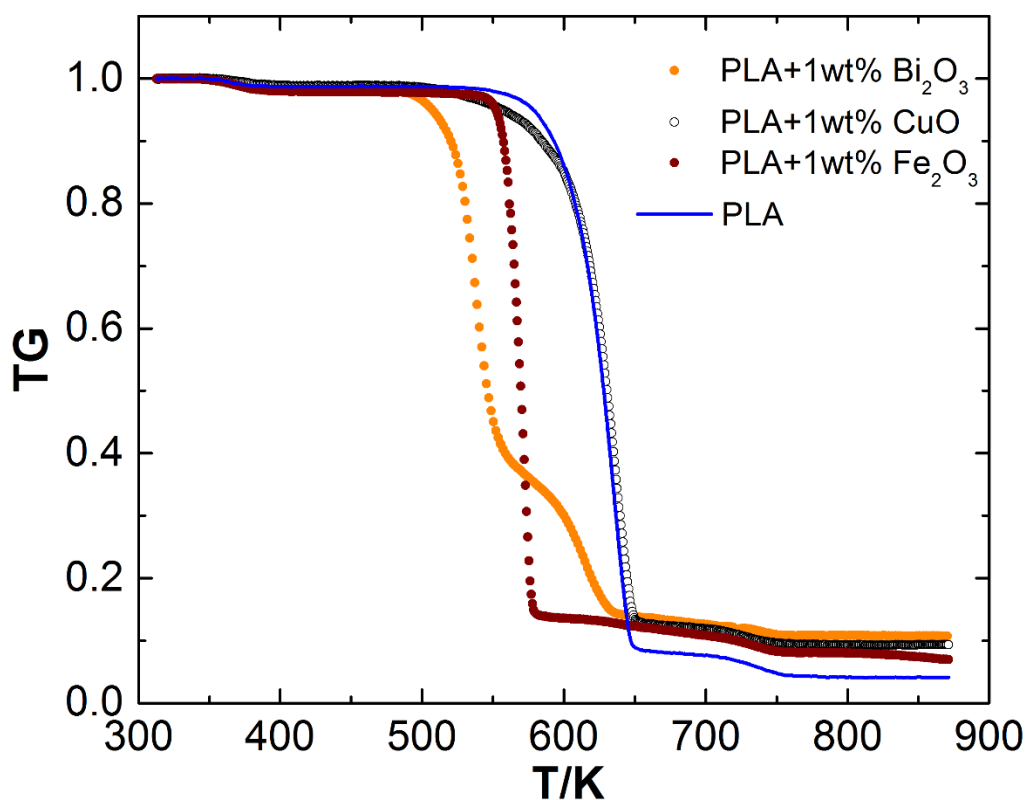
173

174

175

Figure 5 shows the TGA data of thermal decomposition mass loss under N<sub>2</sub> inert atmosphere. It is clear that the various types of MO additives affect the thermal stabilities of PLA/MOs differently, which can also be clearly seen in Figure 6 from Derivative Thermogravimetry (DTG) experimental curves (dotted lines). Specifically, the onset thermal degradation temperature for neat PLA as a reference is approximately  $T_{5\%} \approx 580$  K. For PLA/Bi<sub>2</sub>O<sub>3</sub>, this temperature is 75 K lower ( $T_{5\%} \approx 505$  K), while the effect of Fe<sub>2</sub>O<sub>3</sub> is about 30 K decrease ( $T_{5\%} \approx 550$  K) compared to neat PLA; CuO shows no noticeable effect. The thermal degradation temperatures at maximum weight loss ( $T_{max}$ ), are 536 K (614 K for the second peak),

176 573 K, 634 K and 635 K for PLA/ $\text{Bi}_2\text{O}_3$ , PLA/ $\text{Fe}_2\text{O}_3$ , PLA/ $\text{CuO}$  and neat PLA respectively. These  
177 results show that the catalytic properties trend as:  $\text{Bi}_2\text{O}_3 > \text{Fe}_2\text{O}_3 > \text{CuO}$ . While the DSC signals  
178 reveal notable differences at the stage of decomposition, the addition of MOs does not significantly  
179 affect the melting point  $\sim 425$  K or the heat of melting (as seen in DSC Figure 7). The heats of  
180 melting (the first peak integrals) are within 4% difference of their mean.

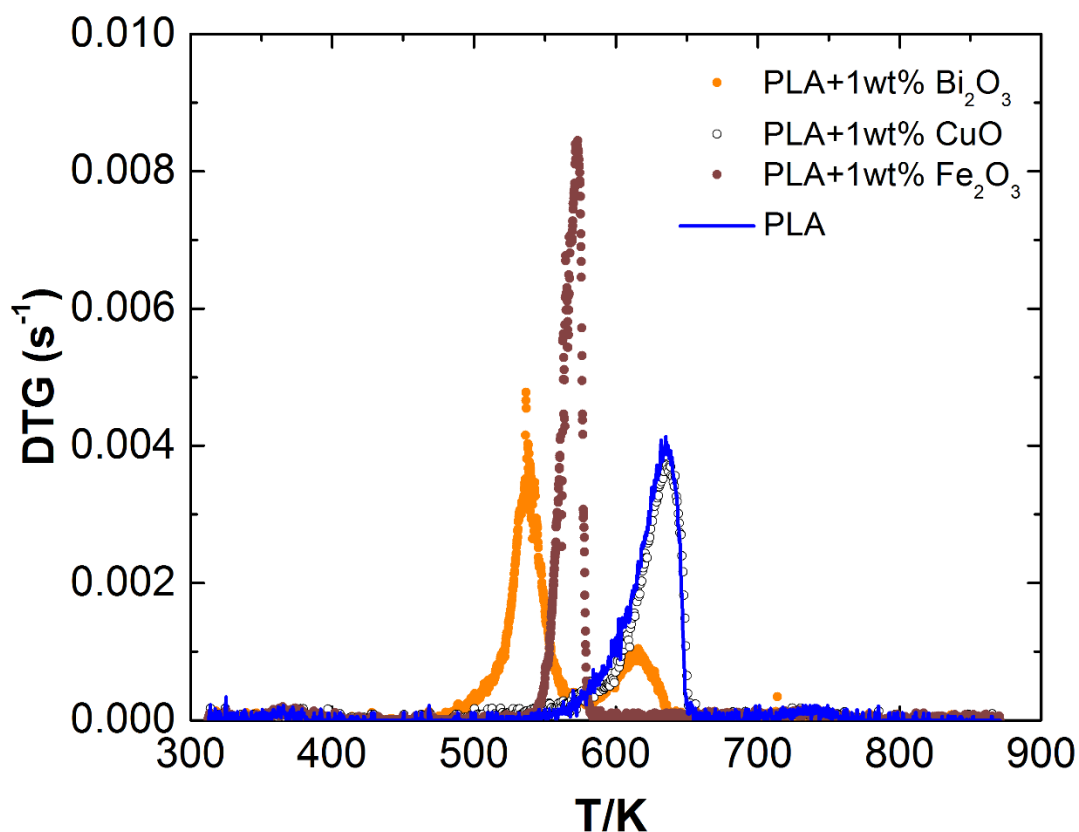


181

182

**Figure 5.** TGA of PLA and PLA/MOs.





183

184

**Figure 6.** DTG plots of PLA and PLA/MOs.

185

186

187

188

189

190

191

192

To better evaluate the decomposition kinetics at various heating conditions and scales, which are necessary as fundamentals to predict the catalytic effects of the MOs on the PLA decomposition, we have extracted phenomenological rate parameters using a numerical pyrolysis software - ThermaKin.<sup>20</sup> ThermaKin solves the mass and energy conservation equations numerically for one or two dimensional objects exposed to external (convective and/or radiative) heat. In this study, we use the thermally thin mode to simulate the thermal degradation processes inside the STA furnace. The material of the object (sample) is described by multiple components, which may interact chemically and physically. The neat PLA and PLA/MOs kinetics were

193 characterized using the methodology reported in our recent publications.<sup>23</sup> This methodology has  
194 been successfully applied to reproduce TGA and DSC signals of 15 non-charring and charring  
195 polymers.<sup>23,24</sup> The resulting kinetic parameters were also shown to predict gasification or burning  
196 rates of these polymers at a wide range of thermal conditions.<sup>23-26</sup>

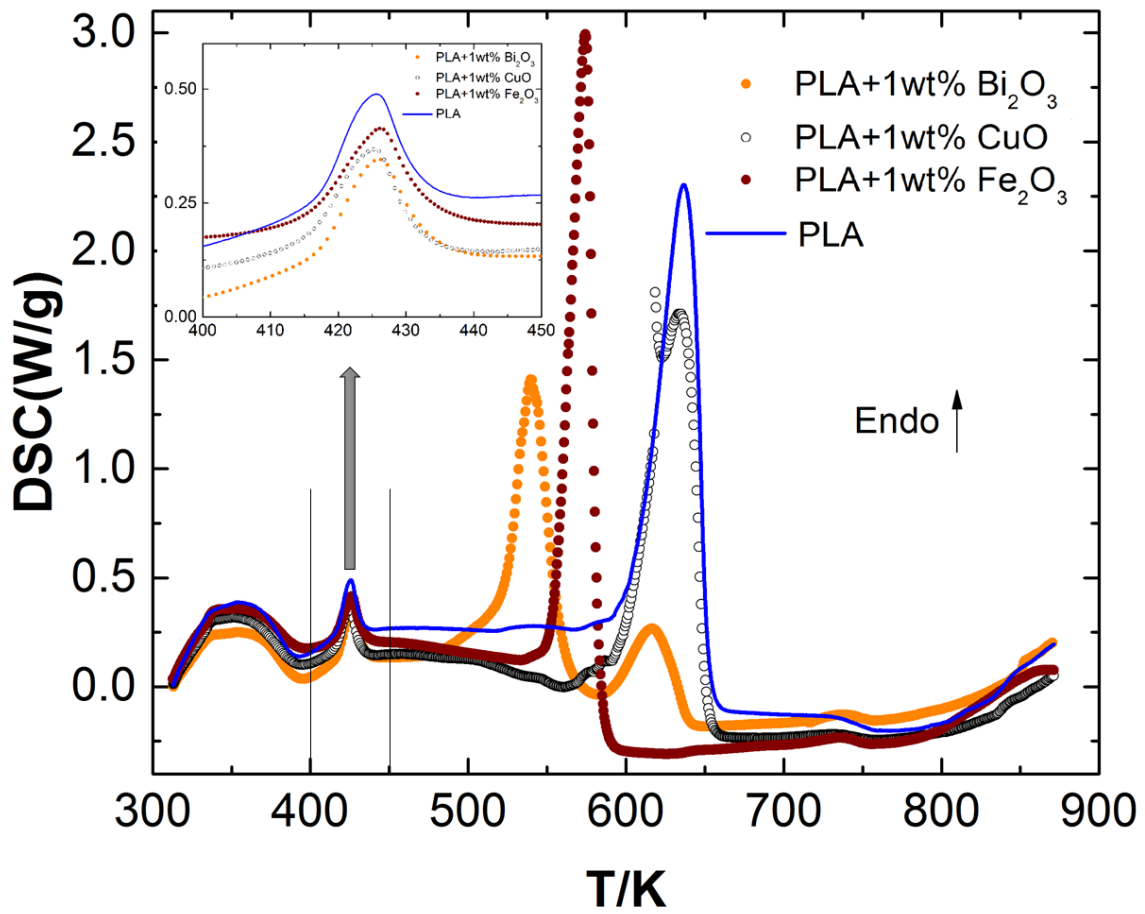
197 In the previous study, neat PLA was tested using STA and the kinetics of its decomposition  
198 was modeled using two consecutive first order reactions.<sup>23</sup> One more reaction was employed to  
199 describe melting ( $T_{\text{melt}} = 425$  K). This was done to use a minimum number of parameters to  
200 describe the entire time-resolved TGA and DSC curves. The kinetics of those reactions are  
201 parameterized with Arrhenius parameters ( $A_x$ ,  $E_x$  represent decomposition reaction  $x$ ; while  $A_m$ ,  
202  $E_m$  represent the melting) listed in Table 1. The value of the  $\theta_x$  is calculated by the instantaneous  
203 mass (at the end stage of the reaction  $x$ ) over its initial mass. Note that the  $\theta_x$ , obtained directly  
204 from the TGA experiments, corresponds to the remaining condensed phase residue yielded in the  
205 reaction  $x$ . Those parameters are initially estimated using simple analytical expressions<sup>27</sup> and then  
206 changed in small increments following the rules summarized in the previous studies until  
207 agreements with the experiment is reached (based on preset coefficient of determination and visual  
208 comparison). Each model reaction corresponds to tens or, perhaps, hundreds of elementary  
209 chemical processes operating within the same range of temperatures.

210 The MOs do not affect the phase transition as evident from DSC curves in Figure 7 (enlarged  
211 temperature range in the left corner). The kinetic parameters describing the melting were reported  
212 previously<sup>23</sup>. For all the PLA composites, MOs are found to affect the thermal degradation process  
213 significantly, which is apparent in both the TGA and DSC measurements. The impact of MOs on  
214 the kinetics of decomposition is quantified through changes in the parameters of the first (major)  
215 reaction. The kinetic parameters are summarized in Table 1. With the exception of PLA/Bi<sub>2</sub>O<sub>3</sub>,

216 the decomposition of all composites can be described by two consecutive reactions. The kinetics  
217 of the second reaction remain unaffected by the addition of MOs. In the case of PLA/Bi<sub>2</sub>O<sub>3</sub>, the  
218 thermal decomposition process consists of three consecutive reactions reflecting a more complex  
219 DTG signal. It has been widely concluded that the thermal decomposition of pure PLA is a one-  
220 stage reaction that involves the loss of ester groups in pure nitrogen<sup>28</sup> and air<sup>29, 30</sup>, consistent with  
221 our observations for neat PLA and PLA/CuO in this study. Other researchers have also observed  
222 multiple reaction steps with the addition of other catalysts<sup>6</sup>, although little information on  
223 mechanism is available. Our speculation for the existing second peak is that part of the PLA  
224 remains unaffected by the catalytic Bi<sub>2</sub>O<sub>3</sub> during the first decomposition step, and it decomposes  
225 as neat PLA at a higher temperature to form the second peak. Further investigation is required to  
226 validate this hypothesis.

227 For all the materials, the solid lines in Figure 8 represent the numerical simulation results  
228 from the ThermaKin. All the simulation results fit the experimental data well and the calculated  
229 coefficients of determination of the experimental data and the fitted curves are all above 0.9.

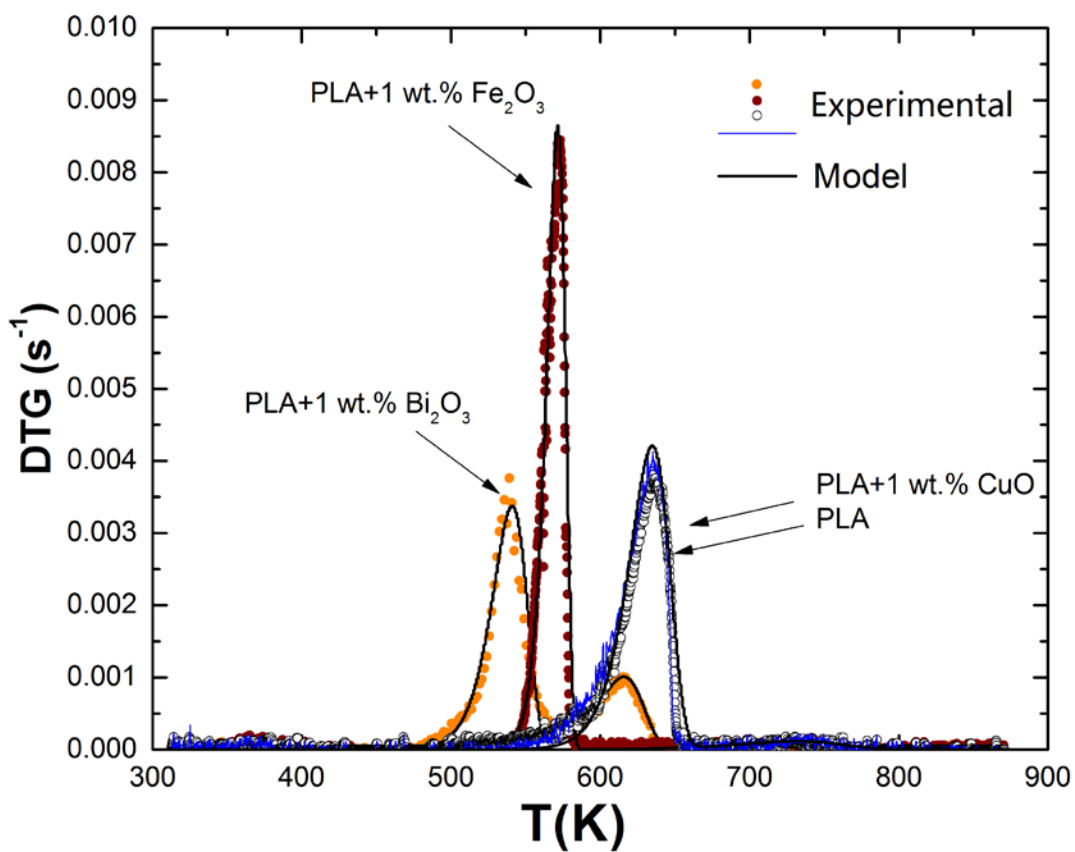




230

231

Figure 7. DSC test of PLA and PLA/MOs.



232

233 **Figure 8.** Experimental and simulated DTG of PLA & PLA/MO composites at 10 K min<sup>-1</sup>.

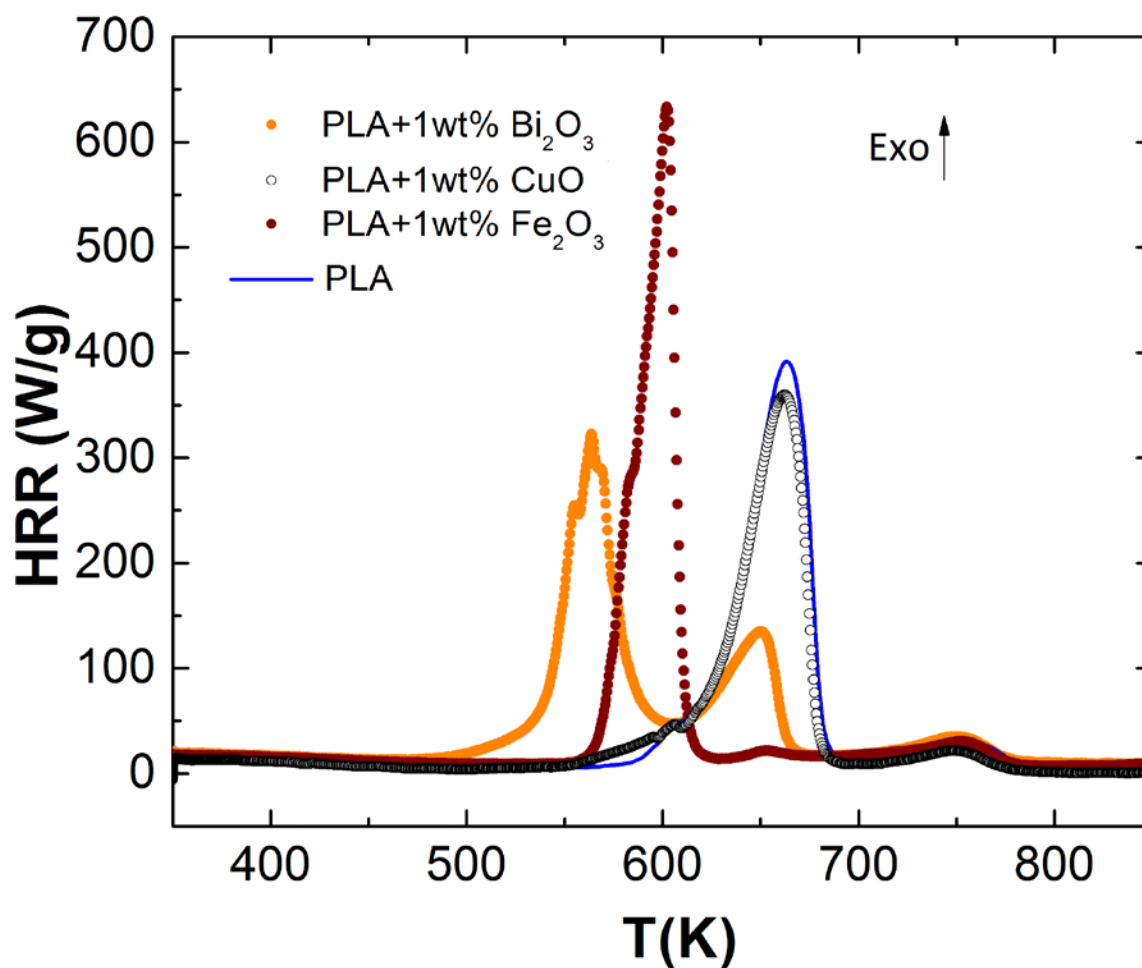
234

Polymer	$A_1$ (s <sup>-1</sup> )	$E_1$ (kJ mol <sup>-1</sup> )	$\theta_1$	$A_2$ (s <sup>-1</sup> )	$E_2$ (kJ mol <sup>-1</sup> )	$\theta_2$	$A_3$ (s <sup>-1</sup> )	$E_3$ (kJ mol <sup>-1</sup> )	$\theta_3$	$A_m$ (s <sup>-1</sup> )	$E_m$ (kJ mol <sup>-1</sup> )
PLA	1.68E18	245	0.1	4.58E6	126	0.4	N/A	N/A	N/A	6.0E40	355
PLA+ Fe <sub>2</sub> O <sub>3</sub>	1.80E38	436	0.14	4.58E6	126	0.5	N/A	N/A	N/A	6.0E40	355

PLA+ Bi <sub>2</sub> O <sub>3</sub>	1.34E18	207	0.38	2.85E15	205.5	0.37	4.58E6	126	0.72	6.0E40	355
PLA+ CuO	1.68E18	245	0.1	4.58E6	126	0.4	N/A	N/A	N/A	6.0E40	355

235 Table 1 Kinetic parameters for PLA, PLA/Fe<sub>2</sub>O<sub>3</sub>, PLA/Bi<sub>2</sub>O<sub>3</sub> and PLA/CuO.

236 The Heat Release Rate(HRR) is measured by MCC, as shown in the Figure 9. The heat  
237 release rate curves for all the PLA/MOs composites match the reaction peaks of TGA and DSC  
238 qualitatively but not quantitatively with respect to their peak temperatures. The corresponding heat  
239 release rate peaks in Figure 9 for all the samples shift to a higher temperature by approximately 27  
240 ~ 28 K compared to the DTG and DSC results in Figures 6 & 7.



241

242

**Figure 9** HRR of PLA, PLA/Fe<sub>2</sub>O<sub>3</sub>, PLA/Bi<sub>2</sub>O<sub>3</sub> and PLA/CuO.

243

244

245

246

247

248

This temperature difference is caused by the relatively higher heating rate (60 K min<sup>-1</sup>) utilized in the MCC compared to the heating rate (10 K min<sup>-1</sup>) in the STA test. The integral of the heat release rate, which accounts for the heat of combustion of the gaseous decomposition products, is approximately equal for all tested samples yielding 19.5±0.8 kJ/g. Therefore, all of these three types of 1wt% PLA/MOs affect the thermal degradation processes only in the condensed phase but have no effect on the heat of combustion.

249 **4. Conclusion**

250 In this paper, we offer a facile method to incorporate metal oxide additives and evaluate  
251 their catalytic effects on PLA thermal decomposition. More specifically, we have explored Bi<sub>2</sub>O<sub>3</sub>,  
252 CuO and Fe<sub>2</sub>O<sub>3</sub> nanoparticles as catalysts for PLA thermal decomposition. Bi<sub>2</sub>O<sub>3</sub> is shown to be a  
253 highly effective catalyst for PLA thermal decomposition. With only 1wt% loading, it lowered the  
254 onset decomposition temperature (T<sub>5%</sub>) by 75 K and the decomposition temperature at the  
255 maximum weight loss (T<sub>max</sub>) by approximate 100 K, comparable to the most effective catalysts  
256 studied so far. The same amount of Fe<sub>2</sub>O<sub>3</sub> and CuO nanoparticles have moderate and negligible  
257 effects on PLA thermal decomposition processes respectively. The overall catalytic effects of the  
258 three metal oxides trend as: Bi<sub>2</sub>O<sub>3</sub> > Fe<sub>2</sub>O<sub>3</sub> > CuO ≈ inert material.

259 The complete heats of combustion for the PLA/MOs composites have been measured by  
260 MCC, in which 1wt% MO additive catalyzes the thermal degradation processes differently in the  
261 condensed phase, and moreover, have negligible effect on the complete combustion heat in the  
262 gas phase as expected. PLA/MOs decomposition was then quantitatively analysed to extract  
263 Arrhenius parameters for the decomposition kinetics, which offers possible explanations and  
264 predictions to evaluate thermal decomposition kinetics at other heating rate conditions.

265 **5. Acknowledgement**

266 This work was partially supported by faculty research fund from the University of New  
267 Haven. The authors would like to thank Ms. Xi Ding for conducting the MCC tests.

268 **6. Reference**

- 269 1. R. E. Drumright, P. R. Gruber and D. E. Henton, *Advanced Materials*, 2000, **12**, 1841-  
270 1846.  
271 2. Y. Fan, H. Nishida, Y. Shirai, Y. Tokiwa and T. Endo, *Polymer Degradation and Stability*,  
272 2004, **86**, 197-208.

- 273 3. Y. Fan, H. Nishida, T. Mori, Y. Shirai and T. Endo, *Polymer*, 2004, **45**, 1197-1205.  
274 4. C. Gottschalk and H. Frey, *Macromolecules*, 2006, **39**, 1719-1723.  
275 5. M. Kreiger and J. M. Pearce, *ACS Sustainable Chemistry & Engineering*, 2013, **1**, 1511-  
276 1519.  
277 6. H. Dong, A. P. Esser-Kahn, P. R. Thakre, J. F. Patrick, N. R. Sottos, S. R. White and J. S.  
278 Moore, *ACS Applied Materials & Interfaces*, 2012, **4**, 503-509.  
279 7. R. C. R. Gergely, S. J. Pety, B. P. Krull, J. F. Patrick, T. Q. Doan, A. M. Coppola, P. R.  
280 Thakre, N. R. Sottos, J. S. Moore and S. R. White, *Advanced Functional Materials*, 2015,  
281 **25**, 1043-1052.  
282 8. F. Carrasco, P. Pagès, J. Gámez-Pérez, O. O. Santana and M. L. MasPOCH, *Polymer*  
283 *Degradation and Stability*, 2010, **95**, 116-125.  
284 9. L. M. Pitet, M. A. Amendt and M. A. Hillmyer, *J Am Chem Soc*, 2010, **132**, 8230-8231.  
285 10. T. S. Coope, U. F. J. Mayer, D. F. Wass, R. S. Trask and I. P. Bond, *Advanced Functional*  
286 *Materials*, 2011, **21**, 4624-4631.  
287 11. T. Mori, H. Nishida, Y. Shirai and T. Endo, *Polymer Degradation and Stability*, 2004, **84**,  
288 243-251.  
289 12. H. Zhang, J. Huang, L. Yang, R. Chen, W. Zou, X. Lin and J. Qu, *RSC Advances*, 2015, **5**,  
290 4639-4647.  
291 13. S.-Z. Guo, F. Gosselin, N. Guerin, A.-M. Lanouette, M.-C. Heuzey and D. Therriault,  
292 *Small*, 2013, **9**, 4118-4122.  
293 14. S.-z. Guo, X. Yang, M.-C. Heuzey and D. Therriault, *Nanoscale*, 2015, **7**, 6451-6456.  
294 15. H. A. Reed, C. E. White, V. Rao, S. Ann, B. Allen, C. L. Henderson and P. A. Kohl, *J.*  
295 *Micromech. Microeng.*, 2001, **11**, 733-737.  
296 16. S. Metz, S. Jiguet, A. Bertsch and P. Renaud, *Lab on a Chip*, 2004, **4**, 114-120.  
297 17. C. Wu, K. Sullivan, S. Chowdhury, G. Jian, L. Zhou and M. R. Zachariah, *Advanced*  
298 *Functional Materials*, 2012, **22**, 78-85.  
299 18. G. Jian, L. Liu and M. R. Zachariah, *Advanced Functional Materials*, 2013, **23**, 1341-1346.  
300 19. L. Liu and M. R. Zachariah, *Energy & Fuels*, 2013, **27**, 4977-4983.  
301 20. S. I. Stoliarov and R. E. Lyon, *Thermo-Kinetic Model of Burning*, Federal Aviation  
302 Administration Technical Note, 2008.  
303 21. ASTM(D7309-13), *Standard Test Method for Determining Flammability Characteristics*  
304 *of Plastics and Other Solid Materials Using Microscale Combustion Calorimetry 7309*,  
305 2013.  
306 22. W. Thornton, *Philosophical Magazine and J. of Science*, 1917, **33**, 196-203.  
307 23. J. Li and S. I. Stoliarov, *Combust Flame*, 2013, **160**, 1287-1297.  
308 24. J. Li, J. Gong and S. I. Stoliarov, *Int J Heat Mass Tran*, 2014, **77**, 738-744.  
309 25. J. Li and S. I. Stoliarov, *Polymer Degradation and Stability*, 2014, **106**, 2-15.  
310 26. J. Li, J. Gong and S. I. Stoliarov, *Polymer Degradation and Stability*, 2015, **115**, 138-152.  
311 27. R. E. Lyon, R. N. Walters and S. I. Stoliarov, *Journal of ASTM International*, 2006, **3**, 1-  
312 18.  
313 28. M. A. G. Cristian-Andi Nicolae, Raluca Augusta Gabor, *Engineering Letter*, 2008, **16**.p568  
314 29. M. C. G. a. V. G. Deshmukh, *Coll Polym. Sci.*, 1982, **260**, 514-517.  
315 30. M. C. G. a. V. G. Deshmukh, *Coll. Polym. Sci*, 1982, **260**, 308-311.

---